Original Article

Computational analysis on transient MHD free convection flow in a microchannel in presence of inclined magnetic field with Hall and ion slip current

Basant K Jha[1] and Peter B Malgwi[2] (iD)

Abstract

The present analysis is concerned with the effect of magnetic field inclination on transient MHD flow of Newtonian viscous fluid in a vertical microchannel with the consideration of Hall and ion slip currents as well as induced magnetic field effects. Obtained dimensional partial differential equation are rendered dimensionless by employing suitable parameters and thereafter solved numerically in MATLAB. Relevant actions of parameters on different flow features are depicted explicitly and also using Tables for various applicable parameters. Analysis in this direction is relevant in many MHD controlled applications. Results obtained from the present analysis shows that at the early stages of time and in the simultaneous occurrence of inclined magnetic field as well as Hall and ion slip currents, velocity and induced magnetic field behavior are found to be oscillatory all through the microchannel domain.

Introduction

Recently, interest has been drawn to the theoretical/ numerical analysis involved in the study of transient magnetohydrodynamic flow in different channel geometries. This is owing to its vast practical application in many engineering application, few of such can be found in nuclear engineering, generation and transmission of electricity in MHD devices, electromagnetic heating, sensor application, biomedical application, aerodynamics, plasma industries amongst others. Several theoretical/numerical studies related with time dependent hydromagnetic flow exist in the literature. Georgantopoulos[1] presented an analysis of hydromagnetic buoyancy driven flow of conducting fluid past an accelerated permeable surface. Kim[2] investigated on the time dependent hydromagnetic flow of polar fluid past through a permeable surface with porous material. Sahoo et al.[3] studied on time dependent MHD buoyancy driven flow past a long plate taking into consideration the influence of heat generation/ absorption. Ferdows et al.[4] presented the similarity solution for hydromagnetic flow in permeable surface.

Singha and Deka[5] examined the influence of shear stress on time dependent flow through heated parallel plates. Seddeek and Salama[6] discussed on the influence of temperature dependent viscosity and thermal conductivity on time dependent hydromagnetic flow through a permeable surface with porous material. Kumar et al.[7] numerically presented a study on transient hydromagnetic buoyancy driven flow in a semiinfinite permeable plate with heat source and suction using the Crank-Nicolson scheme. They reported that higher values of magnetic field augment temperature profile whereas it decrease with a rise in heat generation. Other notable related articles on the subject can

[1]Department of Mathematics, Ahmadu Bello University, Zaria, Nigeria
[2]Department of Mathematics, Air Force Institute of Technology, Kaduna, Nigeria

Corresponding author:
Peter B Malgwi, Department of Mathematics, Air Force Institute of Technology, Kaduna 810107. Nigeria.
Email: bumalpeter@gmail.com

be seen in: Jha et al.,[8] Jha and Apere,[9] Singh,[10] and Reddy and Yaragani.[11]

Research has also shown that in the study of magnetohydrodynamics, the inclusion of induced magnetic field due to the dynamic movement of conducting fluid in the occurrence of magnetic field has a wide range of application in the field of engineering, manufacturing and space science. Taking into account the inclusion of induced magnetic field in MHD flow equations: Kumar and Singh[12] discussed the influence of induced magnetic field on time dependent buoyancy driven flow of conducting fluid through a single plate surface. Kumar and Singh[13] also presented an analytical study on influence of induced magnetic field on free convection flow with the inclusion of Newtonian heating/cooling between two concentric cylinders. In a related work, Sarveshanand and Singh[14] presented an analysis on the influence of induced magnetic field on free convection flow of conducting fluid between two parallel walls. Recently, Mollah and Islam[15] presented a numerical study on transient heat transfer of compressible conducting fluid through a permeable surface considering the influence of induced magnetic field. Jha and Aina[16] discussed the influence of induced magnetic field on MHD free convection in a permeable system. They reported that in the occurrence of a permeable microchannel, there exist regions where the influence of magnetic field be insignificant on magnetic induction. In another related work, Jha and Aina[17] point out that in the situation where one of the microchannel wall is anticipated to be electrically conducting, higher values of magnetic field retards shear stress significantly.

Recent study of MHD flow has shown that the inclusion of the combined effect of Hall and ion slip current on MHD flow equations becomes adequate if the conducting fluid is situated in the existence of a strong applied magnetic field. Practical significance of including the Hall term in the MHD flow equations is that it induces secondary velocity in the flow field which is an important features of coriolis force (Suttong and Sherman[18] and Sato[19]). Application of MHD flow with the inclusion of the Hall and ion slip term could be seen in Hall actuators, Hall probes, magnetic sensors, transducers amongst others. Therefore, it becomes of interest to investigate the combined influence of Hall and ion slip current on MHD flow problems. Kumar et al.,[20] discussed the influence of Hall current on MHD buoyancy driven flow in the occurrence of an induced magnetic field. They reported that introducing Hall current augment velocity profile whereas it retards magnetic induction. In a related work, Kumar et al.,[21] discussed the significance of Hall current as well as wall conductance effect on MHD flow. They reported that introducing Hall current in the occurrence of a conducting wall augment velocity as well as the induced magnetic field profile. Seth and Singh[22] examined the influence of Hall current on pressure driven flow in a revolving channel

with wall conductance effects. Other relevant articles on the subject can be found in Jha et al.,[23] Jha and Malgwi,[24,25] Singh et al.,[26] Dwivedi and Singh,[27] Krishna,[28,29] Krishna et al.,[30] Mahmud et al.,[31] also presented a study on the role of Hall current on magnetic shear thinning flow of nanofluid. Sharma and Shaw[32] examined the role of viscous dissipation and non – linear radiation on magnetohydrodynamic flow of non-Newtonian fluid past a stretching sheet. Sharma et al.[33] presented an analysis on unsteady hydromagnetic flow of non-Newtonian fluid past a stretching surface with binary chemical reaction. Sharma and Mishra[34] demonstrated the role of micro rotation on hydromagnetic for the control of radiative heat as well as thermophoretic influence. Tinker et al.,[35] presented a numerical simulation for unsteady radiative flow of hybrid nanofluid. Interesting recent articles on this type of flow can be found.[36–65]

Inspired by the above works, the present research is dedicated to investigate on the transient magnetohydrodynamic flow of Newtonian viscous fluid in a vertical microchannel with induced magnetic field as well as Hall and ion slip currents. The influence of inclined magnetic field is taken into consideration. Previous, studies on MHD flow in the vicinity of a strong magnetic field inducing Hall and ion slip currents have anticipated the applied magnetic field to be normal to the conducting fluid. However, in many practical applications such as in MHD power generator, the applied magnetic field can be found to be inclined. The significance of an inclined magnetic field could be beneficial in establishing the optimum performance and improving the operation in MHD devices. The novelty of the present research is the consideration of an inclined magnetic field on MHD flow of Newtonian viscous fluid in a vertical microchannel with Hall and ion slip currents as well as induced magnetic field effects. Several studies have discussed the influence of an inclined magnetic field on hydromagnetic flow in the occurrence of Hall current. Ghosh[66] examined the influence of inclined magnetic field on MHD Couette flow through a revolving channel with Hall current. In a related work, Ghosh et al.[67] studied on influence of oblique magnetic field on time dependent hydromagnetic natural and pressure driven flow of conducting fluid in a channel. Bég et al.[68] presented a numerical study on the influence of inclined magnetic field and Hall current on revolving hydromagnetic flow using finite element and network electrical simulation. They reported that in the occurrence of an inclined magnetic field, higher values of Darcy number augment velocity profiles whereas higher values of Hall current retards primary velocity and augments secondary velocity. Other related works can be found in Jha and Malgwi.[69] A computational analysis is developed and the effects of dimensionless time, Hall and ion slip current, induced magnetic field as well as orientation of the applied magnetic field on conducting
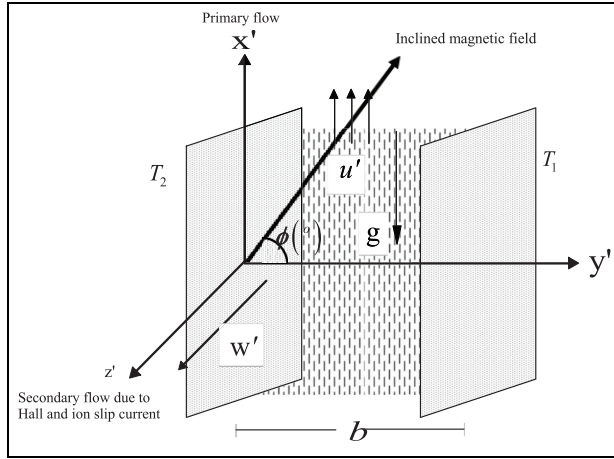
Figure 1. Flow geometry.

fluid is considered. Such analysis have thus, not been accounted for in the scientific literature.

Mathematical analysis

Flow geometry of the problem under consideration is illustrated in Figure 1. Consider the time dependent hydromagnetic free convection flow through a microchannel induced magnetic field. The applied magnetic field is anticipated to be inclined at an angle (ϕ) and the influence of Hall and ion slip are taken into attention. The gap between microchannel walls are anticipated to be "b" distance apart and the walls of the microchannel are anticipated to be electrically insulated. Flow coordinate is anticipated such that the direction of flow is taken along the straight vertical x'-axis whereas the y'-axis taken normal to it (See Figure 1). Initially at $t' \leqslant 0$, it is assumed that the fluid, microchannel walls are at temperature T_0. Thereafter at $t' > 0$, the temperature at the right microchannel wall situated at $y' = b$ is raised to T_1 while the temperature at microchannel wall $y' = 0$ is kept at T_2 with $T_1 > T_2$ giving rise to free convection current. It is also assumed that the imposed magnetic field is taken to be large to induce Hall and ion slip current in a direction perpendicular to the electric and the imposed magnetic field. Following Jha and Malgwi,[25,69] the governing flow equations together with initial and boundary conditions are given in dimensional form as:

$$\frac{\partial u'}{\partial t'} = \upsilon \frac{\partial^2 u'}{\partial y'^2} + \frac{\mu_e H_0' cos(\phi)}{\rho} \frac{\partial H_x'}{\partial y'} + g\beta(T' - T_0), \tag{1}$$

$$\frac{\partial w'}{\partial t'} = \upsilon \frac{\partial^2 w'}{\partial y'^2} + \frac{\mu_e H_0' cos(\phi)}{\rho} \frac{\partial H_z'}{\partial y'}, \tag{2}$$

$$\frac{\partial H_x'}{\partial t'} = \upsilon_m(1 + \beta_h \beta_i cos(\phi)) \frac{\partial^2 H_x'}{\partial y'^2}$$
$$- \beta_h \upsilon_m cos(\phi) \frac{\partial^2 H_z'}{\partial y^2} + H_0' cos(\phi) \frac{\partial u'}{\partial y'}, \tag{3}$$

$$\frac{\partial H_z'}{\partial t'} = \upsilon_m(1 + \beta_h \beta_i cos(\phi)) \frac{\partial^2 H_z'}{\partial y'^2}$$
$$+ \beta_h \upsilon_m cos(\phi) \frac{\partial^2 H_x'}{\partial y^2} + H_0' cos(\phi) \frac{\partial w'}{\partial y'}, \tag{4}$$

$$\frac{\partial T'}{\partial t'} = \frac{k}{\rho C_p} \frac{\partial^2 T'}{\partial y'^2}, \tag{5}$$

With initial and boundary condition:

$$\left. \begin{array}{l} u'(y', t') = 0 \\ w'(y', t') = 0 \\ H_x'(y', t') = 0 \\ H_z'(y', t') = 0 \\ T'(y', t') = 0 \end{array} \right\} \quad at \quad t' \leqslant 0 \tag{6}$$

At $t' > 0$,

$$u'(y', t') = \frac{2 - f_v}{f_v} \lambda \frac{\partial u'}{\partial y'} \quad w'(y', t') = \frac{2 - f_v}{f_v} \lambda \frac{\partial w'}{\partial y'}$$
$$H_x'(y', t') = 0, \qquad H_z'(y', t') = 0, \qquad at \ y' = 0.$$
$$T'(y', t') = T_2 + \frac{2 - f_t}{f_t} \frac{2\gamma_s}{\gamma_s + 1} \frac{\lambda}{Pr} \frac{\partial T'}{\partial y'} \tag{7}$$

$$u'(y', t') = -\frac{2 - f_v}{f_v} \lambda \frac{\partial u'}{\partial y'}, w'(y', t') = -\frac{2 - f_v}{f_v} \lambda \frac{\partial w'}{\partial y'},$$
$$H_x'(y', t') = 0, \qquad H_z'(y', t') = 0, \qquad at \ y' = b$$
$$T'(y', t') = T_1 - \frac{2 - f_t}{f_t} \frac{2\gamma_s}{\gamma_s + 1} \frac{\lambda}{Pr} \frac{\partial T'}{\partial y'} \tag{8}$$

Introducing the dimensionless quantities:

$$y = \frac{y'}{b}, M = \frac{H_0^2 b}{\nu} \sqrt{\frac{\mu_e}{\rho}}, (u, w) = \frac{(u', w')\nu}{g\beta(T_1 - T_0)b^2},$$
$$(H_x; H_z) = \frac{(H_x'; H_z')\nu}{g\beta b^2(T_1 - T_0)} \sqrt{\frac{\mu_e}{\rho}}, P_m = \nu \sigma \mu_e,$$
$$\upsilon_m = \sigma \mu_e, \quad \theta = \frac{T - T_1}{T_2 - T_1}, \ Pr = \frac{\nu}{\alpha}, \tag{9}$$

Equations (1)–(5) with slip conditions (8) transform to:

$$\frac{\partial u}{\partial t} = \frac{\partial^2 u}{\partial y^2} + Mcos(\phi) \frac{\partial H_x}{\partial y} + \theta, \tag{10}$$

$$\frac{\partial w}{\partial t} = \frac{\partial^2 w}{\partial y^2} + M\cos(\phi)\frac{\partial H_z}{\partial y}, \tag{11}$$

$$\frac{\partial H_x}{\partial t} = (1 + \beta_h\beta_i\cos(\phi))\frac{\partial^2 H_x}{\partial y^2} - \beta_h\cos(\phi)\frac{\partial^2 H_z}{\partial y^2}$$
$$+ MP_m\cos(\phi)\frac{\partial u}{\partial y}, \tag{12}$$

$$\frac{\partial H_z}{\partial t} = (1 + \beta_h\beta_i\cos(\phi))\frac{\partial^2 H_z}{\partial y^2} + \beta_h\cos(\phi)\frac{\partial^2 H_x}{\partial y^2}$$
$$+ MP_m\cos(\phi)\frac{\partial w}{\partial y}, \tag{13}$$

$$\frac{\partial \theta}{\partial t} = \frac{1}{\Pr}\frac{\partial^2 \theta}{\partial y^2}, \tag{14}$$

With slip conditions:

$$\left.\begin{array}{l} u(y,t) = 0 \\ w(y,t) = 0 \\ H_x(y,t) = 0 \\ H_z(y,t) = 0 \\ T(y,t) = 0 \end{array}\right\} \quad at \quad t \leqslant 0 \tag{15}$$

At $t > 0$,

$$u(y,t) = 0. = \beta_v Kn\frac{\partial u}{\partial y}, \quad w(y,t) = \beta_v Kn\frac{\partial w}{\partial y},$$
$$H_x(y,t) = 0, \quad H_z(y,t) = 0, \quad at \quad y = 0 \tag{16}$$
$$\theta(y,t) = \xi + \beta_v KnIn\frac{\partial \theta}{\partial y}$$

$$u(y,t) = -\beta_v Kn\frac{\partial u}{\partial y}, w(y,t) = -\beta_v Kn\frac{\partial w}{\partial y},$$
$$H_x(y,t) = 0, \quad H_z(y,t) = 0 \quad at \quad y = 1 \tag{17}$$
$$\theta(y,t) = 1 - \beta_v KnIn\frac{\partial \theta}{\partial y}.$$

and

$$\beta_v = \frac{2 - f_v}{f_v}, \beta_t = \frac{2 - f_t}{f_t}\frac{2\gamma_s}{\gamma_s + 1}\frac{1}{\Pr}, Kn = \frac{\lambda}{b}, ln = \frac{\beta_t}{\beta_v},$$
$$\xi = \frac{T_2 - T_0}{T_1 - T_0}.$$

Steady state solution

Expression for the steady state for velocity and induced magnetic field are obtained by expressing $\frac{\partial}{\partial t}() = 0$. These solution matches with the result obtained in Jha

and Malgwi[69] where $U = u + iw$, $H = H_x + iH_z$ and presented as follows:

$$U(y) = C_2\cosh(M_1 y) + C_3\sinh(M_1 y) + \frac{A_1}{M_1^2}y - \frac{C_1}{M_1^2}, \tag{18}$$

$$H(y) = \frac{1}{M^2\cos(\theta)}$$
$$\begin{bmatrix} K_{11}M_1\cosh(M_1 y) - C_1(K_8 M_1\sinh(M_1 y) \\ + K_{10}M_1\cosh(M_1 y)) \\ -K_2 - A_0 y - \frac{A_1}{2}y^2 \end{bmatrix} + C_4, \tag{19}$$

$$\Theta(y) = A_0 + A_1 y, \tag{20}$$

Numerical solution

As a result of the coupled nature of the flow equations, it becomes complex to obtain the exact solution to equations (10)–(14), hence we employ a numerical scheme based on the finite difference approximation known as PDEPE in MATLAB to solve the problem as used in Singh et al.[70] The numerical scheme is built for solving parabolic and elliptic partial differential equations.

Numerical values for result presented in this work was independently validated with steady state solution and highlighted in Table 1.

Results and discussion

Dimensionless coupled PDE representing the flow equations (10)–(14) are solved numerically using MATLAB by employing the finite difference method based scheme PDEPE with 0.01 step increment for dimensionless time (t) and distance (y). As stated earlier, the main focus of the present research is to present a computational analysis on transient MHD flow of Hall and ion slip current in a microchannel in the occurrence of induced magnetic field. Therefore, active effects of various flow parameters on velocity, induced magnetic field, induced current density and shear stress are investigated at transient time using graphs and table. In the current work, the thermal surrounding situation of the microchannel walls are assumed under three special case of interest: for the first case, both microchannel walls are anticipated to be heated symmetrically identified as $\xi = 1$. For the second case, the left microchannel wall is anticipated to be not heated or cooled while the right microchannel wall is heated identified as asymmetric heating ($\xi = 0$). And in the third case, the left microchannel wall is anticipated to be cooled while the right microchannel wall is heated identified as asymmetric heating ($\xi = -1$). Furthermore, Figures 2–4 illustrate the 3-D surf plot representing the

Table 1. Numerical comparison for steady state values for velocity profile in the present work with those of Mahmud et al.,[31] for $Pr = 0.72, Pm = 1.0, \beta_i = 0.0, \beta_h = 0.5, \beta_v Kn = 0.05, \phi = \frac{\pi}{4}, \xi = 1.0, M = 2$ and $\ln = 1.667$.

| y	t	u (Present work)	u (Steady) Mahmud et al.[31]	w (Present work)	w (Steady state) Mahmud et al.[31]
0.0	0.05	0.0034	0.0250	0.1790e−06	0.0000
	0.1	0.0069	0.0250	−3.1180e−06	0.0000
	0.2	0.0139	0.0250	−0.3160e−04	0.0000
	0.5	0.0234	0.0250	0.0000	0.0000
	1.0	0.0250	0.0250	0.0000	0.0000
0.2	0.05	0.0073	0.1032	2.1120e−06	0.0006
	0.1	0.0218	0.1032	8.0280e−06	0.0006
	0.2	0.0530	0.1032	0.3710e−04	0.0006
	0.5	0.0961	0.1032	0.0004	0.0006
	1.0	0.1031	0.1032	0.0006	0.0006
0.4	0.05	0.0047	0.1409	−2.5210e−06	0.0014
	0.1	0.0241	0.1409	−2.9230e−06	0.0014
	0.2	0.0686	0.1409	1.5990e−04	0.0014
	0.5	0.1308	0.1409	0.0010	0.0014
	1.0	0.1408	0.1409	0.0013	0.0014
0.6	0.05	0.0047	0.1409	−2.5210e−06	0.0014
	0.1	0.0241	0.1409	−2.9230e−06	0.0014
	0.2	0.0686	0.1409	1.5990e−04	0.0014
	0.5	0.1308	0.1409	0.0010	0.0014
	1.0	0.1408	0.1409	0.0013	0.0014
0.8	0.05	0.0073	0.1032	2.1120ee−06	0.0006
	0.1	0.0218	0.1032	8.0280e−06	0.0006
	0.2	0.0530	0.1032	0.3710e−04	0.0006
	0.5	0.0961	0.1032	0.0004	0.0006
	1.0	0.1031	0.1032	0.0006	0.0006
1.0	0.05	0.0034	0.0250	0.1760e−06	0.0000
	0.1	0.0069	0.0250	−3.1180e−06	0.0000
	0.2	0.0139	0.0250	−0.3160e−04	0.0000
	0.5	0.0234	0.0250	0.0000	0.0000
	1.0	0.0250	0.0250	0.0000	0.0000

variation of dimensionless time and distance on velocity, induced magnetic field, and temperature profile.

Figure 5(a) illustrate the computed primary velocity distribution versus the dimensionless time in the occurrence of induced magnetic field (IMF), and an inclined magnetic field. Under these situations, the thermal conditions of the microchannel walls are assumed to be either with the same ambient temperature or heated asymmetrically. As expected, higher values of dimensionless time leads to higher values of velocity profiles for $\xi = 1$ and $\xi = 0$ heating situations. This could be attributed to stronger buoyancy current associated with symmetric heating. In the situation where $\xi = -1$, a dual character is observed for velocity as dimensionless time increases. Hence, higher values of dimensionless time augment velocity toward the heated wall whereas a reverse flow is noticed toward the cold wall. Observation from Figure 5(b) however reveals that higher values of dimensionless time causes an oscillatory behavior along the secondary flow direction when $\xi = 1$ and $\xi = 0$. Cooling the left microchannel wall and increasing the dimensionless time cancels out the oscillatory behavior until the peak is attained.

Figure 6(a) and (b) exhibit the influence of induced magnetic field (IMF) with variation of dimensionless time in the occurrence of an inclined magnetic field (ϕ), Hall and ion slip currents (β_h, β_i). Observation from Figure 6(a) shows that in the situation where the microchannel walls are electrically insulated, higher values of dimensionless time augment IMF when $\xi = 0$ and $\xi = -1$ yielding an increase in IMF. In a situation where the both microchannel walls are heated simultaneously, corresponding to $\xi = 1$, higher values of dimensionless time augment the IMF toward the left microchannel wall whereas it retards it toward the right wall. Based on this observation, it is interesting to conclude that at transient time, the IMF in microchannel could be optimized or controlled by changing the thermal surrounding condition of the microchannel. The opposite flow behavior is noticed for IMF along the induced flow direction (see Figure 6(b)).

Variation of velocity and induced magnetic field (IMF) with inclined magnetic field parameter (ϕ) is highlighted in Figures 7 and 8 at transient time. Illustration from Figure 7(a) reveals that in the existence of Hall and ion slip currents, higher values of ϕ has almost no significant influence on main component of velocity for all values of ξ. However as the secondary component is observed, higher values of ϕ leads to an oscillatory flow behavior all through the microchannel domain. For symmetric heating ($\xi = 1$), higher values of ϕ augments velocity toward the heated microchannel
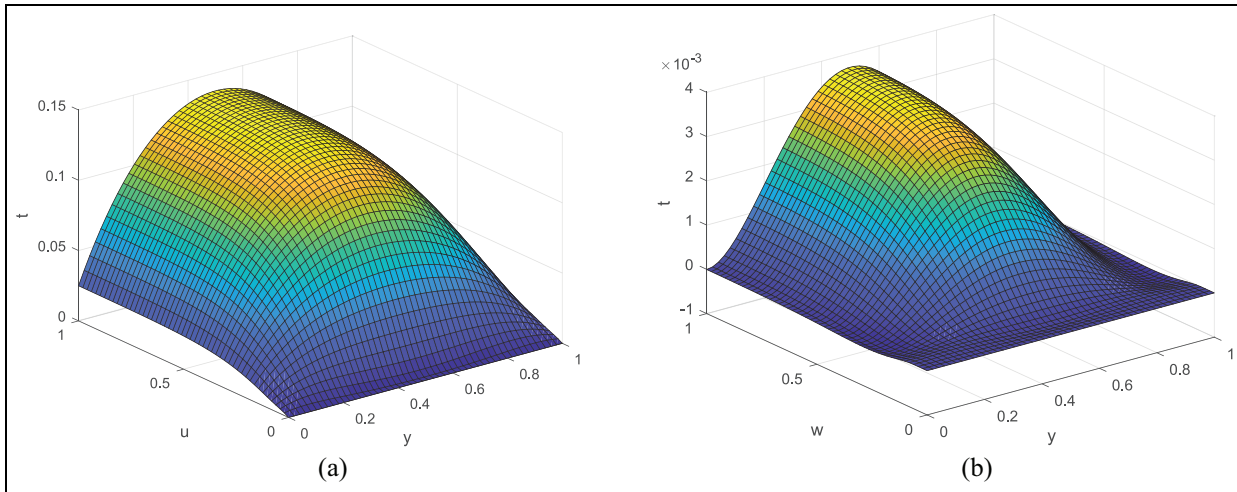
Figure 2. (a) Primary and (b) secondary velocity profile with dimensionless time (*t*) and distance (*y*).
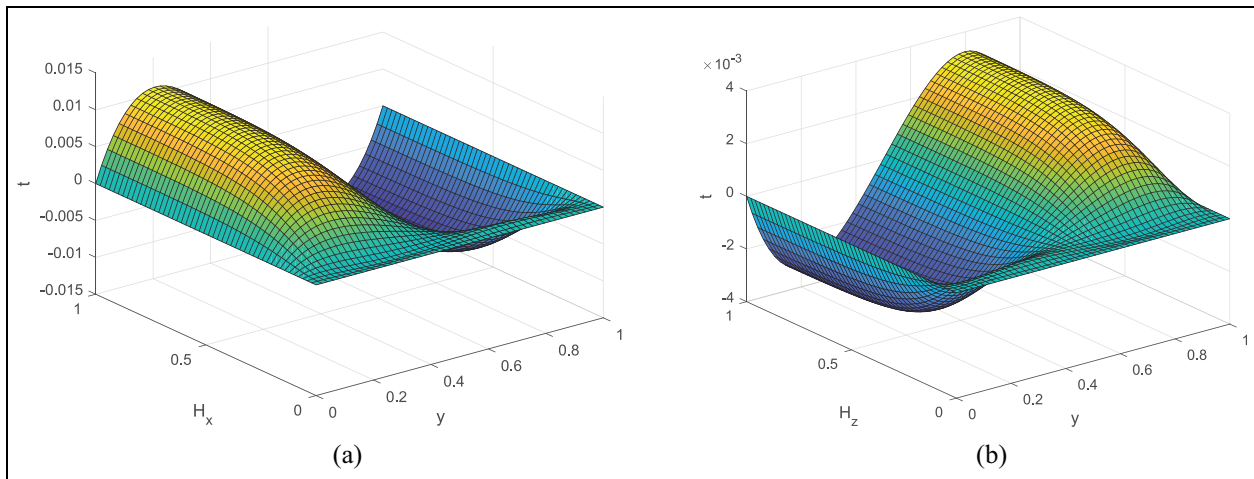

Figure 3. (a) Primary and (b) secondary IMF profile with dimensionless time (*t*) and distance (*y*).

walls whereas it destabilizes it about the center of the channel leading to reverse flow behavior. This could be attributed to stronger buoyancy current about the heated microchannel walls causing an observable increase in velocity. Though not displayed, it is also interesting to mention here that changing the orientation of the magnetic field to $\phi = \frac{\pi}{2}$ that is, 90°, implies the magnetic field is placed parallel to the flow and microchannel walls, it is observed that velocity profile cancel out and no flow is induced. However, as the orientation ϕ is increased to $\phi = \pi$, that is, 180°, this corresponds to the physical situation when the magnetic field is placed in the opposite direction along the positive $y - axis$. It is interesting to mention that velocity is maximum about the center of the microchannel whereas it is minimum in a region close to the heated microchannel walls. Hence, we conclude that at transient time, reverse flow behavior can be minimized by changing the orientation of the applied magnetic field.

Figure 8(a) and (b) shows the induced magnetic field (IMF) profiles at transient time for different values of inclined magnetic field parameter (ϕ). Figure 8(a) demonstrate that at transient time, higher values of ϕ weakens magnetic induction (H_x) along the primary direction for $\xi = 0 and \xi = -1$ leading to decrease in IMF. For $\xi = 1$, unlike in other thermal situation, the IMF displays a dual character with higher values of ϕ. Hence, higher values of magnetic inclination augment the IMF toward the heated left microchannel wall while it retards it toward the other wall. Furthermore, magnetic induction is observed to be higher in the case of asymmetric heating $\xi = -1$ in comparison with other heating situations. From this, we can infer that at transient time, the production of induced magnetic field in a microchannel could be optimized or controlled by changing the thermal boundary situation on the microchannel walls as well as the orientation of the applied magnetic field. In the case of secondary IMF, higher
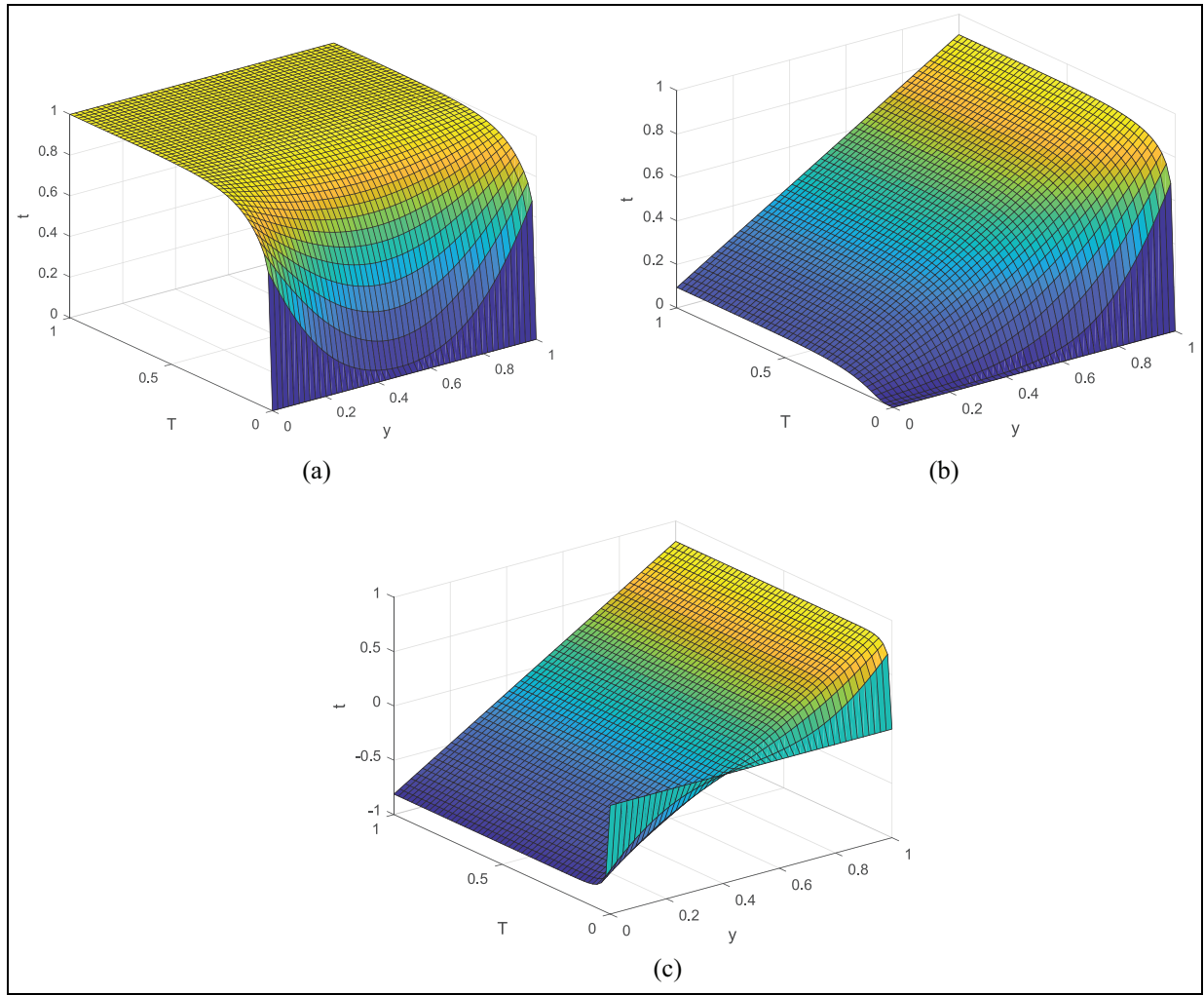
Figure 4. (a and b) Temperature for $\xi = 1.0$ and $\xi = 0.0$ with dimensionless time (t) and distance (y) and (c) temperature for $\xi = -1.0$ with dimensionless time (t) and distance (y).
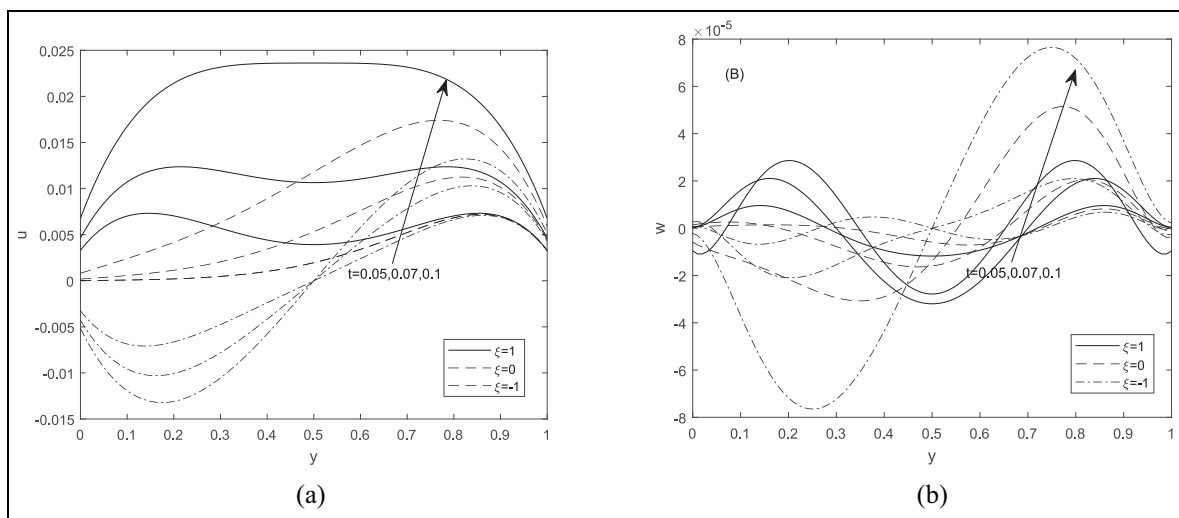
Figure 5. (a) Primary velocity and (b) secondary velocity with dimensionless time: $\beta_h = 0.5, \beta_i = 0.1, Pm = 0.5, \beta_v Kn = 0.05, M = 5$.

amplitude of oscillation is observed with higher values of magnetic inclination parameter (ϕ) which is not true in the case of primary IMF. Furthermore, a detail inspection also shows that induced magnetic field reversal is recorded close to the right microchannel wall for all considered values of ξ. Changing the orientation of
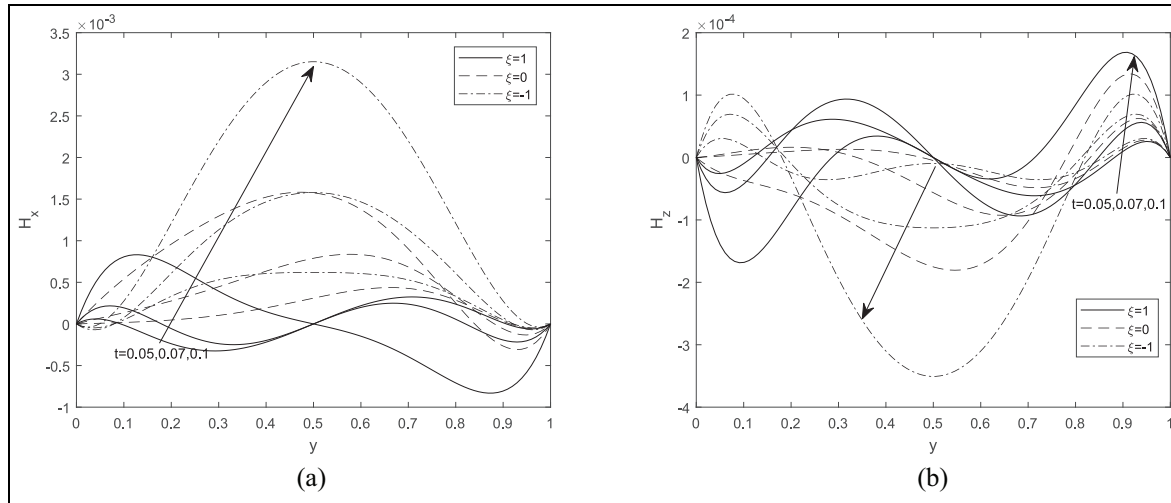
Figure 6. (a) Primary IMF and (b) secondary IMF with dimensionless time: $\beta_h = 0.5, \beta_i = 0.1, Pm = 0.5, \beta_v Kn = 0.05, M = 5, \phi = \pi/4$.

Figure 7. (a) Primary and (b) secondary velocity with magnetic field inclination parameter: $\beta_h = 0.5, \beta_i = 0.1, Pm = 0.5$, $\beta_v Kn = 0.05, M = 5, t = 0.05$.

the magnetic field (ϕ) however, minimizes the induced magnetic field reversal (see Figure 8(b)).

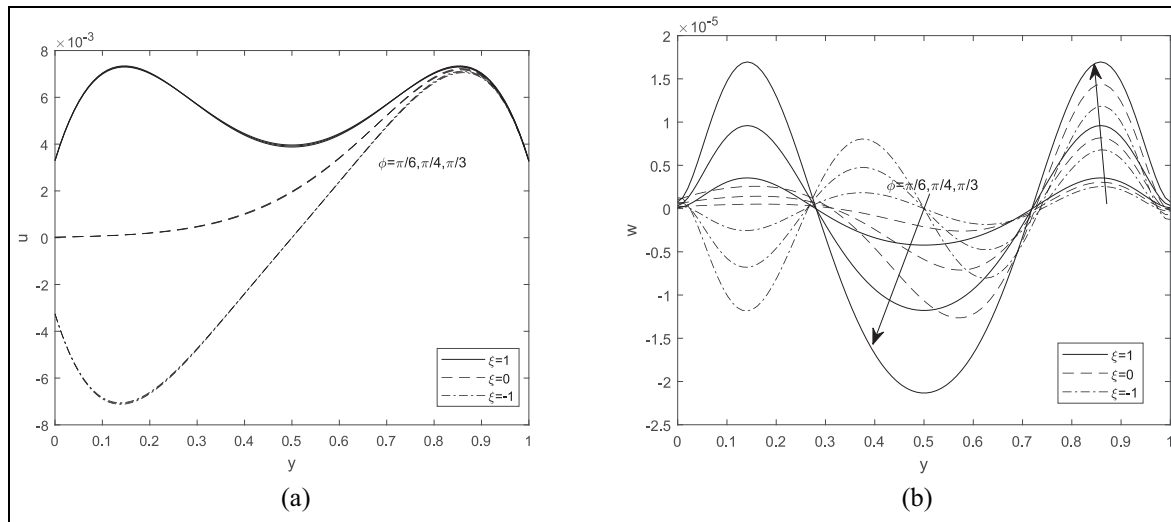In Figure 9(a) and (b), we have displayed the variation of velocity profiles with ion slip parameter (β_i) for three cases of ξ. Figure 9(a) shows that at transient time, higher values of ion slip parameter has almost no significant influence on velocity profile for all considered thermal situation of the microchannel. In the case of secondary velocity (Figure 9(b)), on the other hand it is interesting to mention that higher amplitude of oscillation is recorded with higher values of ion slip parameter. This behavior is true for symmetric and asymmetric heating conditions. Hence, higher values of β_i retards velocity about the microchannel walls whereas it increase about the center of the microchannel. This is expected, as the influence of ion-slip current on velocity is found to be more pronounced in the case secondary velocity in comparison to primary velocity

profile, since Hall and ion slip current are the root cause of the secondary flow.

Variation of IMF with different values of ion slip parameter (β_i) is highlighted in Figure 10(a) and (b) at transient time. Illustration from Figure 10(a) reveal that in the case of primary induced magnetic field, higher values of ion slip parameter causes a slight decrease in induced magnetic field for symmetric and asymmetric heating. The peak is recorded when the left microchannel walls is been cooled in comparison with other cases. In the case of the secondary IMF (Figure 10(b)) unlike the primary IMF, it is evident that magnetic field reversal is observed in a region close to the right microchannel wall for symmetric and asymmetric heating, the magnitude of the magnetic field reversal is reduced by increasing the strength of β_i.

Effects of Hall current parameter on transient velocity profile in the occurrence of inclined magnetic field
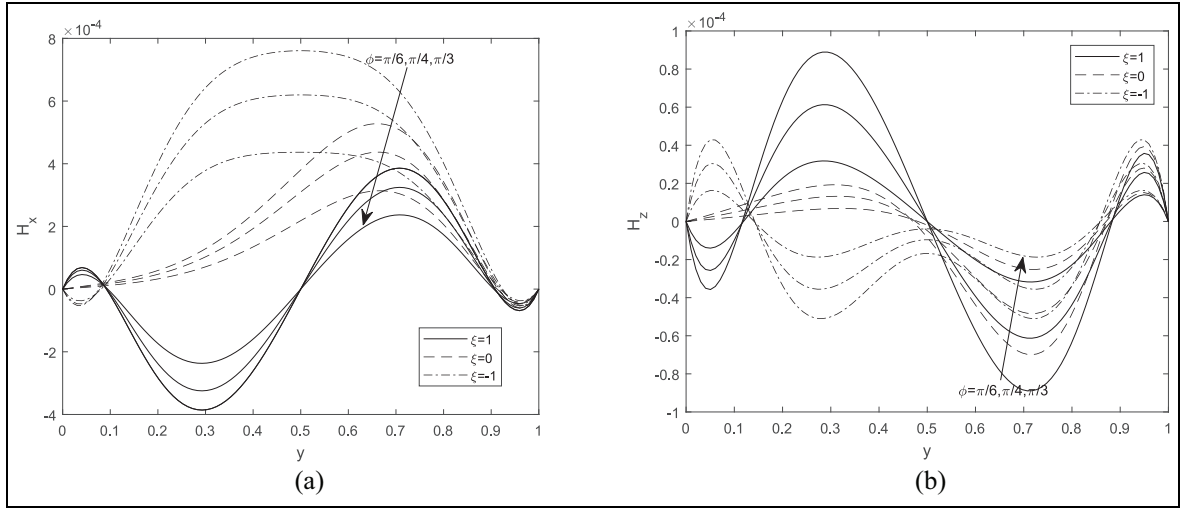
Figure 8. (a) Primary IMF and (b) secondary IMF with magnetic field inclination parameter: $\beta_h = 0.5, \beta_i = 0.1, Pm = 0.5, \beta_v Kn = 0.05$, $M = 5, t = 0.05$.
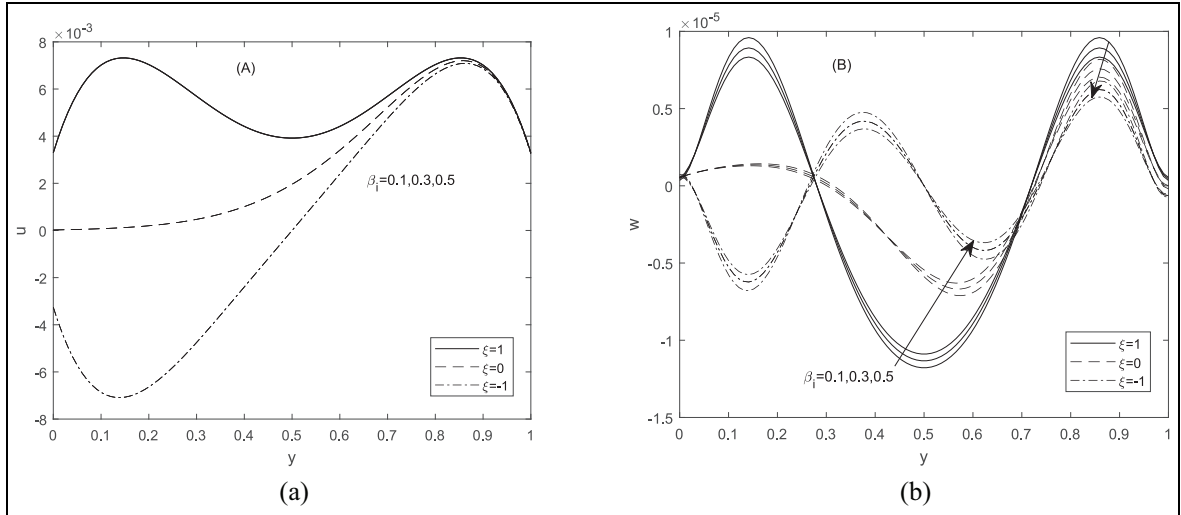
Figure 9. (a) Primary velocity and (b) secondary velocity with ion slip parameter: $\beta_h = 0.5, \phi = {}^\pi/_4, Pm = 0.5, \beta_v Kn = 0.05$, $M = 5, t = 0.05$.

is illustrated in Figure 11(a) and (b). As mentioned previously, it is interesting to observe that at transient time, the influence of Hall current parameter on primary velocity is similar with those recorded in Figure 9(a) against ion slip parameter. Hence, velocity profile is almost not affected with variations in Hall current parameter. In the case of secondary velocity however, higher values of Hall parameter (β_h) induces an oscillatory behavior as well as reverse flow for all microchannel heating situation. Higher amplitude of the reverse flow is observed about the center of the microchannel with symmetric heating in comparison with other heating situations. Furthermore, a point of reference is observed within the microchannel where the velocity profile becomes unaffected with variations in Hall current and net velocity becomes zero around that point (see Figure 11(b)).

Figure 12(a) and (b) highlight the influence of Hall parameter (β_h) on induced magnetic field profile (IMF) at transient time. Observation from Figure 12(a) shows that in the occurrence of inclined magnetic field, primary IMF displays a dual character with variations in Hall parameter. For symmetric $(\xi = 1)$ and asymmetric heating $(\xi = -1)$ however, IMF is symmetric about the center of the microchannel. Furthermore, it is interesting to observe that secondary IMF is also found to be symmetric with variations in β_h for $\xi = 1 \, and \, \xi = -1$. When the left wall is neither heated nor cooled, higher values of β_h induces a magnetic field reversal near the right microchannel wall.

Variations in velocity profile with different values of Hartmann number (M) in the occurrence of magnetic inclination $\left(\phi = \frac{\pi}{4}\right)$ have been depicted in Figure 13(a) and (b) for three special cases of ξ. Figure 13(a) shows
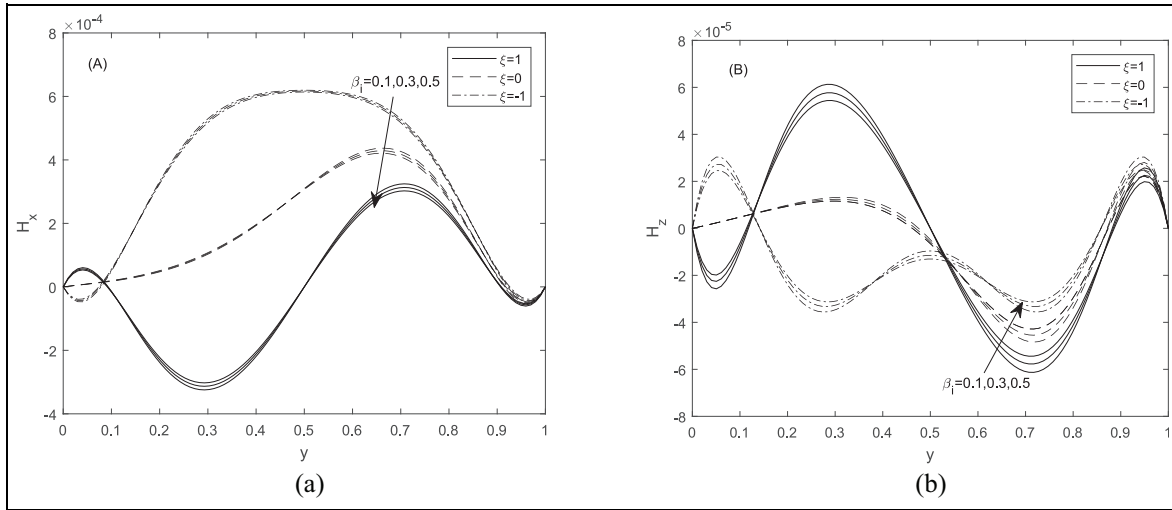
Figure 10. (a) Primary IMF and (b) secondary IMF with ion slip parameter: $\beta_h = 0.5, \phi = \pi/4, Pm = 0.5, \beta_v Kn = 0.05, M = 5, t = 0.05.$

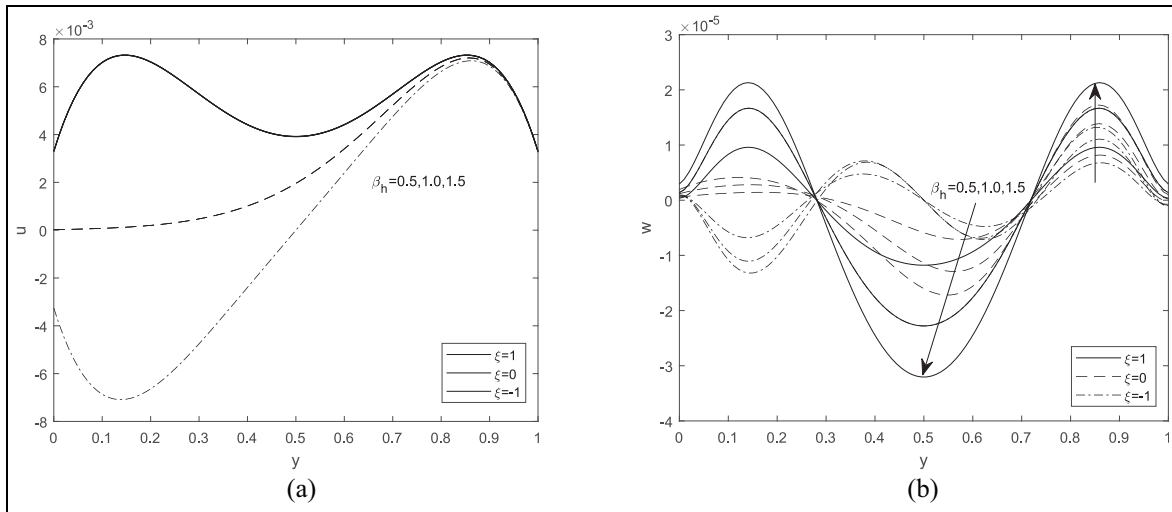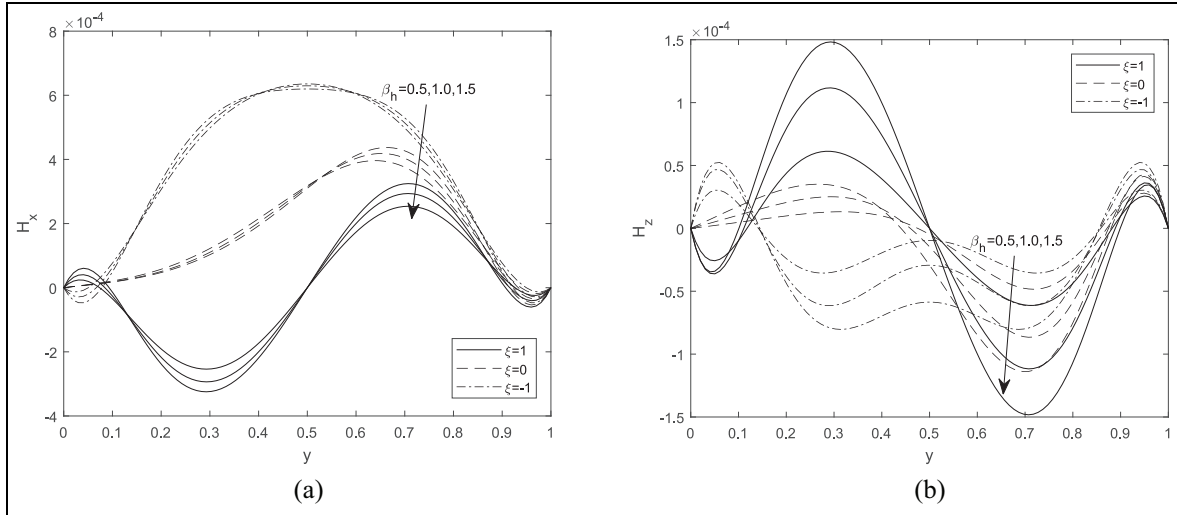**Figure 11.** (a) Primary and (b) secondary velocity with Hall parameter: $\beta_i = 0.1, \phi = \pi/4, Pm = 0.5, \beta_v Kn = 0.05, M = 5, t = 0.05.$

that at transient state, oscillatory flow behavior is observed for symmetric heating ($\xi = 1$), with higher values of Hartmann number however, the oscillatory behavior is almost negligible. Furthermore, the effect of the Hartmann number is to retard the flow near the microchannel walls and stabilize it in the central region. When the left microchannel wall is being cooled ($\xi = -1$) on the contrary, a reverse flow is observed in a region close left wall. Thus indicating a weak convection current. Based on this fact, we infer that at transient time, oscillatory flow and reverse flow behavior could be minimized by increasing the efficiency of the magnetic field as well as heating the microchannel walls simultaneously. Unlike the primary flow, the contrast of this behavior is evident in the case of secondary flow (Figure 13(b)). Illustration from the figure shows that higher amplitude of oscillation is recorded with higher values of Hartmann number which is not true in the case of primary flow.

Influence of Hartmann number on transient IMF in the occurrence of magnetic inclination (ϕ), Hall and ion slip parameter (β_h, β_i) are illustrated in Figure 14(a) and (b). It is interesting to observe from Figure 14(a) that with $\phi = \frac{\pi}{4}$, higher values of Hartmann number support magnetic induction for symmetric heating or otherwise. The peak is observed when the left microchannel wall is being cooled ($\xi = -1$) in comparison with other cases. In addition the IMF is found to be symmetric about the center of the microchannel when the left wall is being cooled (indicating $\xi = -1$). For $\xi = 1$ indicating both walls are being heated, IMF is observed to be asymmetric about the center of the microchannel. Unlike primary IMF, the secondary IMF is found to be oscillatory with variations in Hartmann number. Higher amplitude of oscillation is recorded with higher values of M.

From Table 1, it is noticed that the numerical values for velocity profile in the present work corresponds

Figure 12. (a) Primary IMF and (b) secondary IMF with Hall parameter: $\beta_i = 0.1, \phi = \pi/4, Pm = 0.5, \beta_v Kn = 0.05, M = 5, t = 0.05$.

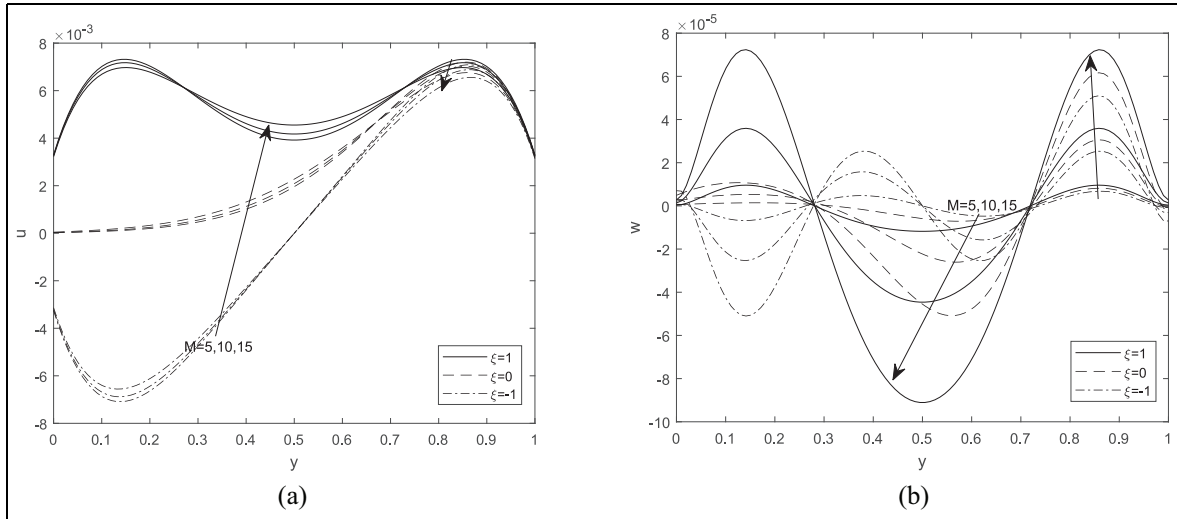**Figure 13.** (a) Primary velocity and (b) secondary velocity with Hartmann number $\beta_i = 0.1, \phi = \pi/4, Pm = 0.5, \beta_v Kn = 0.05$, $\beta_h = 0.5, t = 0.05$.

with those of Mahmud et al.[31] in the instant where the ion slip current is neglected and also the magnetic Prandtl number is taken as unity. These values are obtained by taking higher values of dimensionless time in the present work until steady state is attain.

From Table 2, numerical values for the shear stress (τ_x, τ_z) on both microchannel walls for different values of dimensionless time (t), magnetic field inclination (ϕ), and Hartmann number (M) are illustrated when other flow parameters are kept fixed. It is noticed from the table that irrespective of the value of the inclined magnetic field, higher values of dimensionless time leads to increase in shear stress τ_{x0} whereas it decrease at τ_{x1}. The table also suggest that in the existence of an inclined magnetic field, the influence of Hartmann number on shear stress (τ_x) is more prevalent for $t \leqslant 0.5$ in comparison with other higher values of dimensionless time.

It is observed from Table 3 that in the existence of an inclined magnetic field (ϕ), higher values of dimensionless time (t) augment the primary induced current density (J_x) whereas higher values of magnetic inclination weakens J_x. Based on these behavior, it is interesting to conclude that the induced current density generated in MHD device could be optimized by changing the position of the applied magnetic field.

Table 4 shows that irrespective of the microchannel surrounding temperature (ξ), the rate of heat transfer about right microchannel wall (Nu_1) decrease with higher values of dimensionless time (t) and rarefaction parameter ($\beta_v Kn$) thereby augmenting the temperature profile whereas it increase at (Nu_0).

Table 5 analyzed the impact of Hall (β_h), ion slip (β_i), dimensionless time (t) and magnetic inclination (ϕ) on volume flow rate (δ_x, δ_z) within the
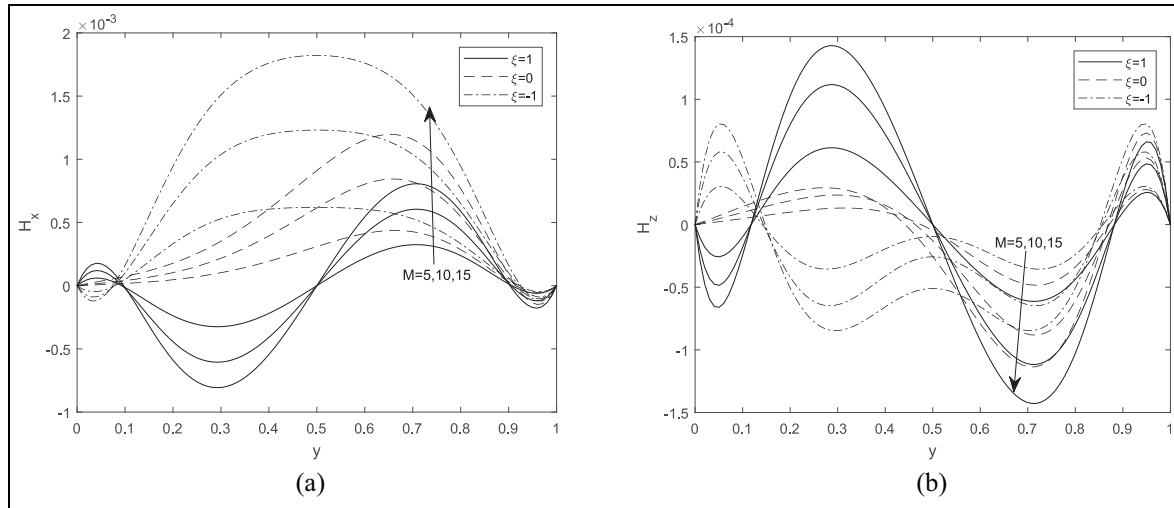
Figure 14. (a) Primary IMF and (b) secondary IMF with magnetic field: $\beta_i = 0.1, \phi = \pi/4, Pm = 0.5, \beta_v Kn = 0.05, \beta_h = 0.5, t = 0.05$.

Table 2. Numerical values for shear stress at $\left(\tau = \frac{\partial U}{\partial y}\right)$ for different flow parameters at microchannel walls $y = 0$ *and* $y = 1$ when Pr $= 0.72, Pm = 0.5, \beta_i = 0.1, \beta_h = 0.5, \beta_v Kn = 0.05$, ln $= 1.667$ *and* $\xi = 1.0$.

t	ϕ	M	τ_{x0}	τ_{x1}	τ_{z0}	$-\tau_{z1}$
0.05	$\frac{\phi}{6}$	5	0.0624	-0.0624	4.7500e$-$05	-4.7500e$-$05
		10	0.0613	-0.0613	1.7730e$-$04	-1.7730e$-$04
		15	0.0599	-0.0599	3.5250e$-$04	-3.5250e$-$04
	$\frac{\phi}{4}$	5	0.0625	-0.0625	2.5720e$-$05	-2.5720e$-$05
		10	0.0618	-0.0618	9.8390e$-$05	-9.8390e$-$05
		15	0.0607	-0.0607	2.0490e$-$04	-2.0490e$-$04
	$\frac{\phi}{3}$	5	0.0626	-0.0626	9.0320e$-$06	-9.0320e$-$06
		10	0.0623	-0.0623	3.5350e$-$05	-3.5350e$-$05
		15	0.0616	-0.0616	7.6680e$-$05	-7.6680e$-$05
0.1	$\frac{\phi}{6}$	5	0.1320	-0.1320	-2.3490e$-$04	2.3490e$-$04
		10	0.1369	-0.1369	-0.0011	0.0011
		15	0.1446	-0.1446	-0.0027	0.0027
	$\frac{\phi}{4}$	5	0.1315	-0.1315	-1.2480e$-$04	1.2480e$-$04
		10	0.1348	-0.1348	-5.8920e$-$04	5.8920e$-$04
		15	0.1402	-0.1402	-0.0015	0.0015
	$\frac{\phi}{3}$	5	0.1310	-0.1310	4.2940e$-$05	-4.2940e$-$05
		10	0.1326	-0.1326	-1.9130e04	1.9130e04
		15	0.1354	-0.1354	-4.8620e$-$04	4.8620e$-$04
0.5	$\frac{\phi}{6}$	5	0.4652	-0.4652	-0.0012	0.0012
		10	0.4686	-0.4686	-4.8930e$-$04	4.8930e$-$04
		15	0.4666	-0.4666	0.0018	-0.0018
	$\frac{\phi}{4}$	5	0.4644	-0.4644	8.2040e$-$04	-8.2040e$-$04
		10	0.4678	-0.4678	-8.6480e$-$04	8.6480e$-$04
		15	0.4679	-0.4679	5.3520e$-$04	-5.3520e$-$04
	$\frac{\phi}{3}$	5	0.4633	-0.4633	-3.8240e$-$04	3.8240e$-$04
		10	0.4662	-0.4662	-8.0060e$-$04	8.0060e$-$04
		15	0.4681	-0.4681	-5.0670e$-$04	5.0670e$-$04

microchannel domain. It is interesting to observe that at transient time, volume flow rate along the primary flow direction is observed to be insensitive to variation in active flow parameters as the volume flow remains unchanged. For higher values of dimensionless time on the other hand, it is obvious that in the occurrence of an inclined magnetic field, a rise in Hall and ion slip current augment volume flow rate (δ_x, δ_z).

Table 3. Numerical values for induced current density $\left(J = -\frac{\partial H}{\partial y}\right)$ at $y = 0.4$, $y = 0.6$ and $y = 0.8$ for different flow parameters when $Pr = 0.72$, $Pm = 0.5$, $\xi = 1.0$, $\ln = 1.667$, $\beta_h = 0.5$, $\beta_i = 0.1$ and $\beta_v Kn = 0.05$.

y	t	ϕ	J_x	J_z
0.4	0.05	$\frac{\phi}{6}$	−0.0021	4.9010e−04
		$\frac{\phi}{4}$	−0.0018	3.3750e−04
		$\frac{\phi}{3}$	−0.0013	1.7470e−04
	0.1	$\frac{\phi}{6}$	0.0024	9.0040e−05
		$\frac{\phi}{4}$	0.0019	1.1540e−04
		$\frac{\phi}{3}$	0.0013	9.1690e−05
	0.5	$\frac{\phi}{6}$	0.0503	−0.0168
		$\frac{\phi}{4}$	0.0451	−0.0132
		$\frac{\phi}{3}$	0.0355	−0.0079
0.6	0.05	$\frac{\phi}{6}$	−0.0021	4.9010e−04
		$\frac{\phi}{4}$	−0.0018	3.3750e−04
		$\frac{\phi}{3}$	−0.0013	1.7470e−04
	0.1	$\frac{\phi}{6}$	0.0024	9.0040e−05
		$\frac{\phi}{4}$	0.0019	1.1540e−04
		$\frac{\phi}{3}$	0.0013	9.160e−05
	0.5	$\frac{\phi}{6}$	0.0503	−0.0168
		$\frac{\phi}{4}$	0.0451	−0.0132
		$\frac{\phi}{3}$	0.0355	−0.0079
0.8	0.05	$\frac{\phi}{6}$	0.0022	−6.0270e−04
		$\frac{\phi}{4}$	0.0019	−4.1980e−04
		$\frac{\phi}{3}$	0.0019	−0.2200
	0.1	$\frac{\phi}{6}$	0.0031	−0.0015
		$\frac{\phi}{4}$	0.0028	−0.0011
		$\frac{\phi}{3}$	0.0021	−6.2730e−04
	0.5	$\frac{\phi}{6}$	−0.0035	0.0000
		$\frac{\phi}{4}$	−0.0035	0.0004
		$\frac{\phi}{3}$	−0.0032	0.0005

Table 4. Numerical values for Nusselt number $\left(Nu = \frac{\partial \theta}{\partial y}\right)$ at $y = 0$ and $y = 1$ when $Pr = 0.72$ and $\ln = 1.667$, $\beta_v Kn = 0.05$.

ξ	t	$\beta_v Kn$	Nu_0	Nu_1
1.0	0.05	0.0	−2.3263	2.3263
		0.05	−2.1414	2.1414
		0.10	−1.8018	1.8018
	0.07	0.0	−1.7450	1.7450
		0.05	−1.7447	1.7447
		0.10	−1.5457	1.5457
	0.10	0.0	−1.1504	1.1504
		0.05	−1.3167	1.3167
		0.10	−1.2546	1.2546
0.0	0.05	0.0	0.0555	2.3812
		0.05	0.0131	2.1546
		0.10	0.0058	1.8075
	0.07	0.0	0.1997	1.9443
		0.05	0.0664	1.8113
		0.10	0.0322	1.5780
	0.10	0.0	0.4385	1.5888
		0.05	0.1943	1.5109
		0.10	0.1054	1.3599
-1.0	0.05	0.0	2.4368	2.4368
		0.05	2.1678	2.1678
		0.10	1.8134	1.8134
	0.07	0.0	2.1440	2.1440
		0.05	1.8780	1.8780
		0.10	1.6103	1.6103
	0.10	0.0	2.0278	2.0278
		0.05	1.7057	1.7057
		0.10	1.4654	1.4654

Conclusions

Influence of magnetic field inclination on transient magnetohydrodynamic free convection flow of Newtonian viscous fluid in a vertical microchannel in the presence of induced magnetic field as well as Hall and ion slip currents is investigated. The microchannel walls are anticipated to be electrically insulated and heated asymmetrically. The obtained coupled system of dimensionless partial differential equations are numerically solved using PDEPE in MATLAB. Influence of interesting active physical flow parameters are discussed. The present research could be relevant in many MHD applications such as magnetic sensors, MHD generators amongst others. Few relevant findings obtained from the results are:

1. Higher values of dimensionless time augment buoyancy current leading to increase in primary velocity profile whereas an oscillatory behavior is observed along the secondary direction.
2. At transient time, changing the magnetic inclination parameter in the occurrence of Hall and ion slip current has almost no significant influence on primary velocity.
3. At transient time, oscillatory flow behavior along secondary direction could be minimized by increasing the magnetic inclination angle as well as the thermal boundary condition of the microchannel.
4. Oscillatory flow behavior could be minimized by considering higher values of Hartmann number as well as heating both microchannel walls.

Based on the results obtained in this research, it would be interesting to interesting to consider the influence of viscous dissipation and Joule heating on transient MHD flow of Newtonian viscous fluid in a vertical microchannel in the presence of inclined magnetic field, Hall and ion slip currents as well as induced magnetic field. Analysis in this direction could further explain the dynamics of conducting viscous fluid in a microchannel in many MHD controlled applications.

Table 5. Numerical values for the volume flow rate $\left(\delta = \int_0^1 U dy = \delta_x + i\delta_z\right)$ for different flow parameters when $Pr = 0.71, \xi = 0.0, Pm = 0.5, M = 5.0, \beta vKn = 0.05$ and $\ln = 1.667$.

t	ϕ	β_i	β_h	δ_x	..
0.05	$\frac{\phi}{6}$	0.1	0.5	0.0040	$-4.2695e-07$
			1.0	0.0040	$-1.5138e-06$
			1.5	0.0040	$-2.9048e-06$
		0.3	0.5	0.0040	$-5.1563e-07$
			1.0	0.0040	$-1.5636e-06$
			1.5	0.0040	$-2.6725e-06$
	$\frac{\phi}{4}$	0.1	0.5	0.0040	$-2.0161e-07$
			1.0	0.0040	$-7.0960e-07$
			1.5	0.0040	$-1.4391e-06$
		0.3	0.5	0.0040	$-2.4923e-06$
			1.0	0.0040	$-7.7403e-07$
			1.5	0.0040	$-1.4028e-06$
0.1	$\frac{\phi}{6}$	0.1	0.5	0.0116	$7.2553e-06$
			1.0	0.0116	$1.0848e-05$
			1.5	0.0116	$1.3309e-05$
		0.3	0.5	0.0116	$6.5553e-06$
			1.0	0.0116	$9.6831e-06$
			1.5	0.0116	$1.1805e-06$
	$\frac{\phi}{4}$	0.1	0.5	0.0116	$4.0093e-06$
			1.0	0.0116	$6.2627e-06$
			1.5	0.0116	$7.6504e-06$
		0.3	0.5	0.0116	$3.6594e-06$
			1.0	0.0116	$5.5984e-06$
			1.5	0.0116	$6.8785e-06$
0.5	$\frac{\phi}{6}$	0.1	0.5	0.0468	0.0012
			1.0	0.0476	0.0018
			1.5	0.0484	0.0018
		0.3	0.5	0.0469	0.0011
			1.0	0.0478	0.0015
			1.5	0.0484	0.0015
	$\frac{\phi}{4}$	0.1	0.5	0.0477	$7.5303e-04$
			1.0	0.0482	0.0012
			1.5	0.0487	0.0013
		0.3	0.5	0.0478	$6.7721e-04$
			1.0	0.0484	$9.8243e-04$
			1.5	0.0488	0.0011

Declaration of conflicting interests

Funding

ORCID iD

Peter B Malgwi   https://orcid.org/0000-0001-7772-964X

References

1. Georgantopoulos GA. Effects of free convection on the hydromagnetic accelerated flow past a vertical porous limiting surface. *Astrophys Space Sci* 1979; 65(2): 433–441.
2. Kim YJ. Unsteady MHD convection flow of polar fluids past a vertical moving porous plate in a porous medium. *Int J Heat Mass Transf* 2001; 44(15): 2791–2799.
3. Sahoo PK, Datta N and Biswal S. Mangnetohydrodynamics unsteady free convective flow past an infinite vertical plate with constant suction and heat sink. *Indian J Pure Appl Math* 2003; 34(1): 145–155.
4. Ferdows M, Ota M, Sattar A, et al. Similarity solution for MHD flow through vertical porous plate with suction. *J Comput Appl Mech* 2005; 6(1): 15–25.

5. Singha G and Deka PN. Skin-friction for unsteady free convection MHD flow between two heated vertical parallel plates. *Theor Appl Mech* 2006; 33(4): 259–280.

6. Seddeek MA and Salama FA. The effects of temperature dependent viscosity and thermal conductivity on unsteady MHD convective heat transfer past a semi-infinite vertical porous moving plate with variable suction. *J Comput Mater Sci* 2007; 40: 186–192.

7. Kumar A, Varshney CL and Sajjan L. Crank-Nicolson scheme to transient MHD free convective flow through semi-infinite vertical porous plate with constant suction | temperature dependent heat source. In: *Proceedings of the international conference on advances in computing and artificial intelligence*, 2011. ACM. DOI: 10.1145/2007052.2007070

8. Jha BK, Aina B and Isa S. Transient magnetohydrodynamic free convective flow in vertical micro-concentric annuli. *J Nanoeng Nanosyst* 2015; 230(4): 1–12.

9. Jha BK and Apere CA. Time-dependent MHD Couette flow in a porous annulus. *Commun Nonlinear Sci Numer Simul* 2013; 18: 1959–1969.

10. Singh RK. Transient free convective MHD flow through porous medium in slip flow regime. *Taiwan J Math* 2015; 11(5): 52–58.

11. Reddy VR and Yaragani HK. Numerical solution of unsteady MHD flow heat transfer over a stretching surface with suction or injection. *Fluid Dyn Mater Process* 2018; 14(3): 213–222.

12. Kumar A and Singh AK. Effect of induced magnetic field on natural convection in vertical concentric annuli heated/cooled asymmetrically. *J Appl Fluid Mech* 2013; 6: 15–26.

13. Kumar D and Singh AK. Effect of induced magnetic field on natural convection with Newtonian heating/cooling in vertical concentric annuli. *Procedia Eng* 2015; 127: 568–574.

14. Sarveshanand S and Singh AK. Magnetohydrodynamic free convection between vertical parallel porous plates in the presence of induced magnetic field. *Springerplus* 2015; 4: 333–339.

15. Mollah T and Islam MM. Numerical solution for unsteady heat transfer of compressible fluid along a porous plate with induced magnetic field. *Model Meas Control B* 2017; 86: 850–863.

16. Jha BK and Aina B. Magnetohydrodynamic natural convection flow in a vertical micro-porous-channel in the presence of induced magnetic field. *Commun Nonlinear Sci Numer Simul* 2018; 64: 14–34.

17. Jha BK and Aina B. Interplay of electrically conducting and non conducting walls on magnetohydrodynamic mixed convection flow in vertical permeable microchannel in existence of induced magnetic field. *Beni-Suef Univ J Appl Sci* 2018; 7: 317–325.

18. Suttong W and Sherman A. *Engineering magnetohydrodynamics*. New York, NY: McGraw-Hill Book Comp, 1965.

19. Sato H. The Hall effect in the viscous flow of ionized gas between parallel plates under transverse magnetic field. *J Phys Soc Jpn* 1961; 16: 1427–1433.

20. Kumar D, Singh AK and Kumar D. Effect of Hall current on the magnetohydrodynamic free convective flow between vertical walls with induced magnetic field. *Eur Phys J Plus* 2018; 133: 207.

21. Kumar D, Singh AK and Sarveshanand M. Effect of Hall current and wall conductance on hydromagnetic natural convection flow between vertical walls. *Int J Ind Math* 2017; 9(4): 1–11.

22. Seth GS and Singh JK. Mixed convection hydromagnetic flow in a rotating channel with Hall and wall conductance effects. *Appl Math Model* 2016; 40: 2783–2803.

23. Jha BK, Samaila G and Malgwi PB. Adomian decomposition method for combined effect of Hall and ion-slip on mixed convection flow of chemically reacting Newtonian fluid in a microchannel with heat absorption/generation. *Int J Mod Phys C* 2020; 31: 1–20.

24. Jha BK and Malgwi PB. Hall current and ion-slip effects on free convection flow in a vertical microchannel with an induced magnetic field. *Heat Transf Asian Res* 2019; 48: 3812–3830.

25. Jha BK and Malgwi PB. Interplay of conducting and non-conducting walls on hydromagnetic natural convection flow in a vertical micro-channel with Hall current. *Propulsion Power Res* 2021; 10: 155–168.

26. Singh J, Joshi N and Begum S. Unsteady magnetohydrodynamic Couette-Poiseuille flow within porous plates filled with porous medium in the presence of a moving magnetic field with Hall and Ion-slip effects. *Int J Heat Technol* 2016; 34: 89–97.

27. Dwivedi N and Singh AK. Effect of line/point heat source and hall current with induced magnetic field on free convective flow in vertical walls. *Indian J Phys* 2022; 96: 169–179.

28. Veera Krishna M. Hall and ion slip effects on MHD free convective rotating flow bounded by the semi-infinite vertical porous surface. *Heat Transf* 2020; 49: 1920–1938.

29. Veera Krishna M. Hall and ion slip effects on MHD laminar flow of an elastico-viscous (Walter's-B) fluid. *Heat Transf* 2020; 49: 2311–2329.

30. Krishna MV, Chamkha AJ and Reddy RSG. Hall and ion slip effects on MHD rotating flow of elastico-viscous fluid through porous medium. *Int Commun Heat Mass Transf* 2020; 113: 104500.

31. Mahmud K, Mehmood R, Rana S, et al. Flow of magnetic shear thinning nano fluid under zero mass flux and Hall current. *J Mol Liq* 2022; 352(15): 118732.

32. Sharma RP and Shaw S. MHD non – Newtonian fluid flow past a stretching sheet under the influence of non – linear radiation and viscous dissipation. *J Appl Comput Mech* 2022; 8(3): 949–961.

33. Sharma RP, Prakash O, Rashidi I, et al. Nonlinear thermal radiation and heat source effects on unsteady electrical MHD motion of nanofluid past a stretching surface with binary chemical reaction. *Eur Phys J Plus* 2022; 137: 297.

34. Sharma RP and Mishra SR. A numerical simulation for the control of radiative heat energy and thermophoretic effects on MHD micropolar fluid with heat source. *J Ocean Eng Sci* 2022; 7(1): 92–98.

35. Tinker S, Mishra S, Pattnaik P, et al. Simulation of time-dependent radiative heat motion over a stretching/shrinking sheet of hybrid nanofluid: Stability analysis for dual

solutions. *Proc IMechE, Part N: J Nanomaterials, Nanoengineering and Nanosystems* 2022; 236(1–2): 19–30.

36. Mishra SR, Sharma RP, Tinker S, et al. Impact of slip and the entropy generation in a darcy-Forchhimer nanofluid past a curved stretching sheet with heterogeneous and homogenous chemical reactions. *J Nanofluids* 2022; 11(1): 48–57.

37. Mishra SR, Tinker S and Sharma RP. Study of a nonuniform heat source over a Riga plate using *n*th-order chemical reaction on Oldroyd-B nanofluid flow for two-dimensional motion. *Heat Transf* 2022; 51(2): 1257–1274.

38. Sharma RP and Mishra S. Analytical approach on magnetohydrodynamic Casson fluid flow past a stretching sheet via Adomian decomposition method. *Heat Transf* 2022; 51(2): 2155–2164.

39. Sharma RP, Prakash O, Ganji DD, et al. Thermal radiation and magnetic field effects on squeezing motion analysis for Cu–kerosene and Cu–water nanofluids. *Heat Transf* 2022; 51(3): 2383–2400.

40. Sharma RP and Mishra SR. Metal and metallic oxide nanofluid over a shrinking surface with thermal radiation and heat generation/absorption. *J Appl Comput Mech* 2022; 8(2): 557–565.

41. Verma AK, Gautam AK, Bhattacharyya K, et al. Existence of boundary layer nanofluid flow through a divergent channel in porous medium with mass suction/injection. *Sādhanā* 2021; 46: 98.

42. Payad SS, Sandep N and Sharma RP. Impact of cross-diffusion on methanol-based Fe3O4 nanofluid. *Bioint Res Appl Chem* 2020; 11(4): 11499–11508.

43. Khader MM and Sharma RP. A numerical solution of the effect of thermal radiation and non-uniform heat source/sink on unsteady MHD micropolar fluid flow past a stretching sheet by fourth – order predictor – corrector finite difference method. *Math Comput Simul* 2021; 181: 333–350.

44. Kumaran G, Sivaraj R, Prasad VR, et al. Finite difference computation of free magneto-convective Powell-eyring nanofluid flow over a permeable cylinder with variable thermal conductivity. *Phys Scr* 2021; 96: 025222.

45. Mburu ZM, Mondal S, Sibanda P, et al. A numerical study of entropy generation on Oldroyd – B nanofluid flow past a Riga plate. *J Therm Eng* 2021; 7(4): 845–866.

46. Sharma RP. Time-dependent oscillatory MHD flow over a porous vertical sheet with heat source and chemical reaction effects. *Indian J Pure Appl Phys* 2020; 58: 877–884.

47. Devaki P, Rao AS, Sharma RP, et al. Impact of hematocriton the flow of casson fluid in contact with jeffery fluid over a narrow pipe. *Indian J Pure Appl Phys* 2020; 58: 758–768.

48. Jena S, Mishra SR, Pattnaik PK, et al. The nanofluid flow between parallel plates and heat transfer in presence of chemical reaction and porous matrix. *Latin Am Appl Res* 2020; 50(4): 283–289.

49. Tinker S, Mishra SR and Sharma RP. Influence of Soret and Dufour effect on MHD flow over an exponential stretching sheet: a numerical study. *Indian J Pure Appl Phys* 2020; 58: 558–568.

50. Sharma RP, Tinker S, Gireesha BJ, et al. Effect of convective heat and mass conditions in magnetohydrodynamic boundary layer flow with Joule heating and thermal radiation. *Int J Appl Mech Eng* 2020; 25(3): 103–116.

51. Rao PS, Prakash O, Mishra R, et al. The transient free convection magnetohydrodynamic motion of nanofluid over a vertical surface under the influence of radiation and heat generation. *Indian J Geo-Marine Sci* 2020; 49(5): 889–897.

52. Sharma RP, Acharya N and Das K. On the effect of variable thickness and melting heat transfer on magnetohydrodynamic nanofluid flow over a slandering stretching sheet. *Indian J Mar Sci* 2020; 49(4): 641–648.

53. Sharma RP and Mishra SR. Effect of higher order chemical reaction on magnetohydrodynamic micropolar fluid flow with internal heat source. *Int J Fluid Mech Res* 2020; 47(2): 121–134.

54. Prakash Sharma R, Indumathi N, Saranya S, et al. Radiative unsteady rarefied gaseous flow over a stretching sheet with velocity slip and temperature jump effects. *J Indian Math Soc* 2020; 87(3–4): 261–275.

55. Sharma RP, Raju MC, Makinde OD, et al. Buoyancy effects on unsteady MHD chemically reacting and rotating fluid flow past a plate in a porous medium. *Defect Diffus Forum* 2019; 392: 1–9.

56. Krishna PM, Sandeep N and Sharma RP. Computational analysis of plane and parabolic flow of MHD Carreau fluid with buoyancy and exponential heat source effects. *Eur Phys J Plus* 2017; 132: 202.

57. Mohan Krishna P, Sharma RP and Sandeep N. Boundary layer analysis of persistent moving horizontal needle in Blasius and Sakiadis magnetohydrodynamic radiative nanofluid flows. *Nucl Eng Technol* 2017; 49(8): 1654–1659.

58. Das K, Sharma RP and Duari PR. Hydromagnetic rarefied fluid flow over a wedge in the presence of surface slip and thermal radiation. *Int J Appl Mech Eng* 2017; 22(4): 827–837.

59. Saranya S, Ragupathi P, Ganga B, et al. Non-linear radiation effects on magnetic/non-magnetic nanoparticles with different base fluids over a flat plate. *Adv Powder Technol* 2018; 29(9): 1977–1990.

60. Das K, Sharma RP and Sarkar A. Heat and mass transfer of a second grade magnetohydrodynamic fluid over a convectively heated stretching sheet. *J Comput Des Eng* 2016; 3(4): 330–336.

61. Sharma RP and Paul A. Transient natural convection magnetohydrodynamic motion over an exponentially accelerated vertical porous plate with heat source. *Indian J Pure Appl Phys* 2019; 57: 205–211.

62. Maraj EN, Khatoon Z, Ijaz S, et al. Effect of Arrhenius activation energy and medium porosity on mixed convective diluted ethylene glycol nanofluid flow towards a curved stretching surface. *Int Commun Heat Mass Transf* 2021; 129: 105691.

63. Rana S, Mehmood R, Bhatti MM, et al. Swimming of motile gyrotactic microorganisms and suspension of nanoparticles in a rheological Jeffery fluid with Newtonian heating along elastic surface. *J Central South Univ* 2021; 28: 3279–3296.

64. Shaiq S, Maraj EN, Mehmood R, et al. Magnetohydrodynamics radiative dissipative slip flow of hydrogen-oxide (H2O) infused with various shape tungsten, tin, titanium (nanometer) particles over a nonlinear radial stretching surface. *Proc IMechE, Part E: J Process Mechanical Engineering* 2022; 236(3): 953–963.

65. Mehmood R, Tabassum R, Ali MR, et al. Crosswise stream of Cu-H2O nanofluid with micro rotation effects: heat transfer analysis. *Nanomater* 2023; 13(3): 471.
66. Ghosh SK. Effects of hall current on MHD Couette flow in a rotating system with arbitrary magnetic field. *Czech J Phys* 2001; 52: 1–13.
67. Ghosh SK, Beg OA and Narahari M. A study of unsteady rotating hydromagnetic free and forced convection in a channel subject to forced oscillation under an oblique magnetic field. *J Appl Fluid Mech* 2013; 6(02): 213–227.
68. Bég A, Rawat S, Zueco J, et al. Finite element and network electrical simulation of rotating magnetofluid flow in nonlinear porous media with inclined magnetic field and hall currents. *Theor Appl Mech* 2014; 41(1): 1–35.
69. Jha BK and Malgwi PB. Effects of hall current and magnetic field inclination on hydromagnetic natural convection flow in a micro-channel with asymmetric thermal boundary condition. *J Therm Sci Eng Appl* 2020; 12: 1–11.
70. Singh RK, Singh AK, Sacheti NC, et al. On hydromagnetic free convection in the presence of induced magnetic field. *Heat Mass Transf* 2010; 46: 523–529.

Appendix for steady state solution

$$A_0 = \xi + \frac{\beta_v Kn(1 - \xi)}{1 + 2\beta_v Kn \ln}, \quad A_1 = \frac{1 - \xi}{1 + 2\beta_v Kn \ln},$$

$$\frac{M^2 cos^2(\theta)}{1 + imcos(\theta)}, K_1 = \frac{1}{M_1{}^2},$$

$$K_2 = A_1 K_1, K_3 = \beta_v Kn K_2, K_4 = \cosh(M_1)$$
$$+ \beta_v Kn M_1 \sinh(M_1), K_5 = sinh(M_1)$$
$$+ \beta_v Kn M_1 cosh(M_1), K_6 = K_2 + K_3, K_7 = \beta_v$$

$$Kn M_1, K_8 = \frac{K_1 K_5 + K_1 K_7}{K_5 + K_7 K_4},$$

$$K_9 = \frac{K_3 K_5 - K_6 K_7}{K_5 + K_7 K_4}, K_{10} = \frac{K_1 - K_1 K_4}{K_5 + K_7 K_4},$$

$$K_{11} = \frac{K_3 K_4 + K_4}{K_5 + K_7 K_4}, K_{12} = K_8 M_1 sinh(M_1)$$
$$+ K_{10} M_1 cosh(M_1), K_{13} = K_9 M_1 sinh(M_1)$$
$$- K_{11} M_1 cosh(M_1),$$

$$K_{14} = A_0 + \frac{A_1}{2} + K_2, C_1 = \frac{K_{11} M_1 + K_{13} + K_{14} - K_2}{K_{10} M_1 - K_{12}},$$

$$C_2 = C_1 K_8 + K_9, C_3 = C_1 K_{10} - K_{11},$$

$$C_4 = \frac{K_{12}(K_2 - K_{11} M_1) - K_{10} M_1 (K_{13} + K_{14})}{M^2 cos(\theta)(K_{12} - K_{10} M_1)},$$

Notation

b	microchannel width (m)
C_p, C_v	Specific heat at constant pressure and volume respectively, $(Joule(J))kg^{-1}(Kelvin(K))^{-1}$
f_v, f_t	thermal and tangential momentum accommodation coefficient, correspondingly
U	complex velocity (dimensionless $U = u + iw$)
H_0	constant magnetic density
Q	dimensionless volume flow rate
J	current density
g	acceleration due to gravity $(meter(m)(sec(s))^{-2})$
$\vec{H}$	magnetic field vector $(Tesla(T))$
k	thermal conductivity $(Wm^{-1}K^{-1})$
t'	time (dimensionless)
t	time (dimensional)
M	Hartmann number (dimensionless)
Pr	Prandtl number (dimensionless)
T	dimensional temperature (K)
T_1	temperature at right wall (K)
T_2	temperature at left wall (K)
(u', w')	component of velocity along primary and secondary directions (ms^{-1})
(H_x', H_z')	component of induced magnetic field along primary and secondary directions $(Ampere(A)m^{-2})$
IMF	induced magnetic field (dimensionless)
Pm	magnetic Prandtl number (dimensionless)
Kn	Knudsen number (dimensionless variable)
ln	fluid wall interaction parameter (dimensionless variable)

Greek symbols

β	volumetric thermal expansion coefficient (K^{-1})
μ	dynamic viscosity $(kgm^{-1}s^{-1})$
μ_e	magnetic permeability $(Newton(N)A^{-2})$
σ	electrical conductivity of the fluid $(ohm^{-1}m^{-1})$
ρ	fluid density (kgm^{-3})
β_h	Hall parameter (dimensionless variable)
β_i	ion slip current (dimensionless variable)
β_v, β_t	velocity slip, temperature jump (dimensionless variable)
θ	temperature (dimensionless)
γ_s	ratio of specific heat C_p/C_v
τ	dimensionless skin friction
ξ	wall-ambient temperature difference parameter
α	thermal diffusivity
λ	molecular mean free path
υ	kinematic viscosity
ϕ	inclined magnetic field parameter